Signatures of strong gravity and fast motions in the polarization: exact analytical treatment

Vladislav Loktev[1], **Alexandra Veledina**[1], **Juri Poutanen**[1]

[1] University of Turku, Finland

arXiv

Abstract

X-ray emission produced in the innermost parts of the accretion disc of compact objects is expected to be polarized. The polarization signatures are strongly affected by the gravitational field of the compact object and relativistic motions of matter in the disc. Spectral dependence of polarization can be used to estimate black hole mass and spin, and such calculations have been performed using ray tracing algorithm. We introduce a simple method to compute the polarization signatures analytically, not relying on the costly ray tracing techniques. The method works equally well for flat, thick, and warped discs. This approach can be used for fast fitting of the X-ray spectro-polarimetric data, which will become available after the coming launch of the IXPE satellite. We also show that the calculation of the observed flux and polarization parameters can be performed with high accuracy using approximate light-bending (ALB) formulas, lifting the need for the pre-computed tabular models in fitting routines.

Analytical solution for polarization parameters

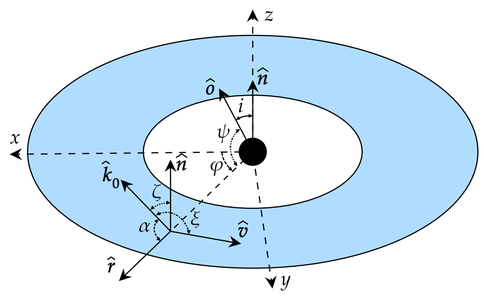

Figure 1: Considered geometry of a flat accretion disc ring. The emitting surface element is described by the radius-vector $\boldsymbol{r}$ and velocity $\boldsymbol{v}$. Vector $\hat{\boldsymbol{o}}$ pointing in the observer direction makes angle i with the normal.

We consider an infinitely thin disc around a massive compact object, as schematically shown in Fig. 1. The general relativity (GR) effect, namely the bending of the light trajectories in the spacetime curved by the compact object, as well as the special relativity (SR) effect due to orbital motion of the matter essentially alter the direction each surface element of the disc is observed from. This affects the observed radiation flux and its polarization properties, namely polarization degree (PD) and polarization angle (PA) χ. For demonstrative reasons, the aforementioned effects on polarization are illustrated by dint of the change in the latter (Figs. 2-6).

In Fig. 2 we show the PA rotation angles due to SR ($\chi^{\rm SR}$), GR ($\chi^{\rm GR}$), and their sum $\chi^{\rm tot}$ as a function of azimuth along the innermost ring of the disc ($r = 3$, r is in units of Schwarzschild radius $R_{\rm S}$.) for different system inclinations. The SR effects are computed for the Keplerian rotation. In general, both the GR and SR rotations decrease with increasing inclination.

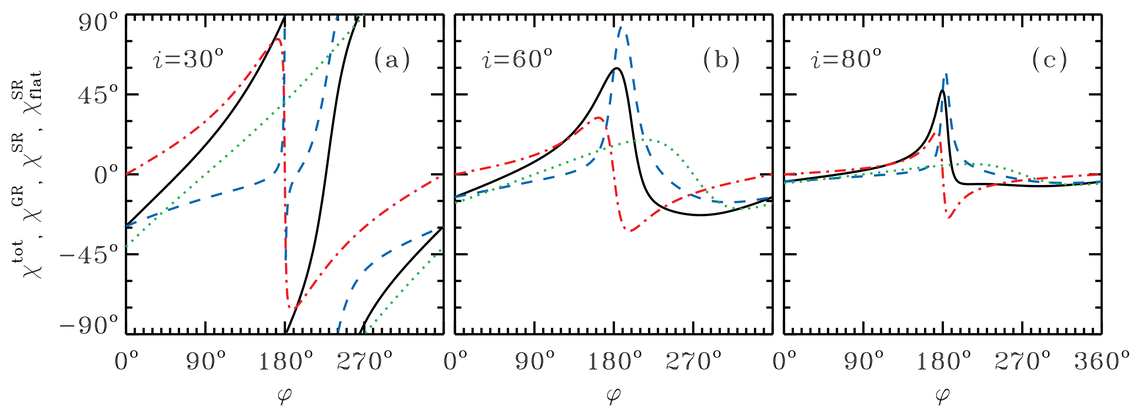

Figure 2: The rotation angles of polarization plane $\chi^{\rm GR}$ (red dot-dashed lines), $\chi^{\rm SR}$ (blue dashed lines), a and $\chi^{\rm SR}_{\rm flat}$, i.e. the rotation due to special relativity if the spacetime were flat, (green dotted lines) and $\chi^{\rm tot} = \chi^{\rm GR} + \chi^{\rm SR}$ (black solid lines) for a ring at $r = 3$ (the innermost segment of the disk) at different viewing angles (*panel a*) $i = 30°$, $60°$ (*b*) and $i = 80°$ (*c*).

Use of light-bending approximation

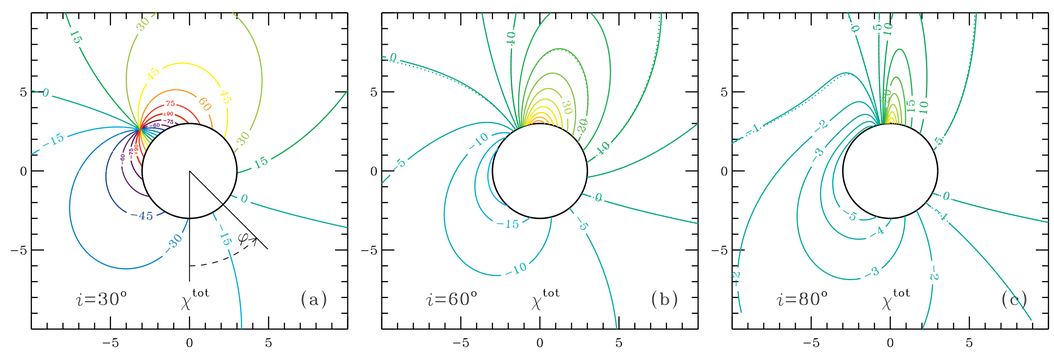

Figure 3: Contours of constant $\chi^{\rm tot}$, i.e. total polarization rotation, at the accretion disc plane (r, φ). The observer is situated at inclinations $i = 30°$ (*panel a*), $60°$ (*panel b*) and $80°$ (*panel c*). The coordinates are in units of Schwarzshild radius $R_{\rm S}$. The polar angle φ is measured from the projection of the direction to the observer on the disc plane. The disc rotates in the counterclockwise direction. The innermost stable circular orbit at $r = 3$ is shown with black circle. The dotted lines (wherever visible) show corresponding contours computed using ALB.

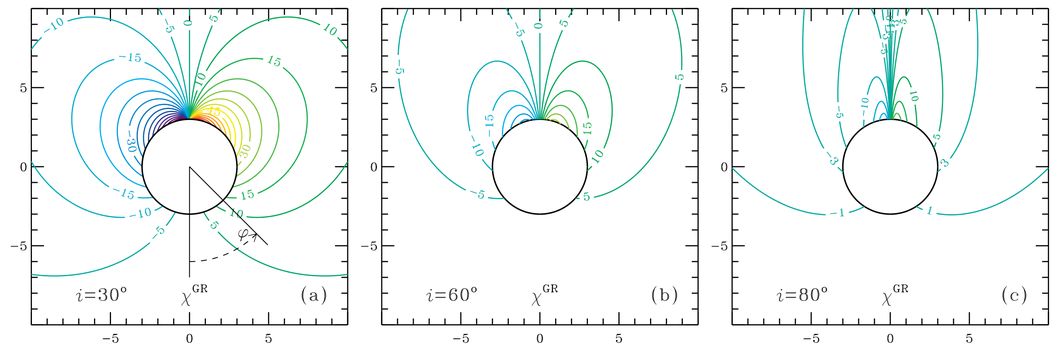

Figure 4: Same as Fig. 3 but for $\chi_{\rm GR}$.

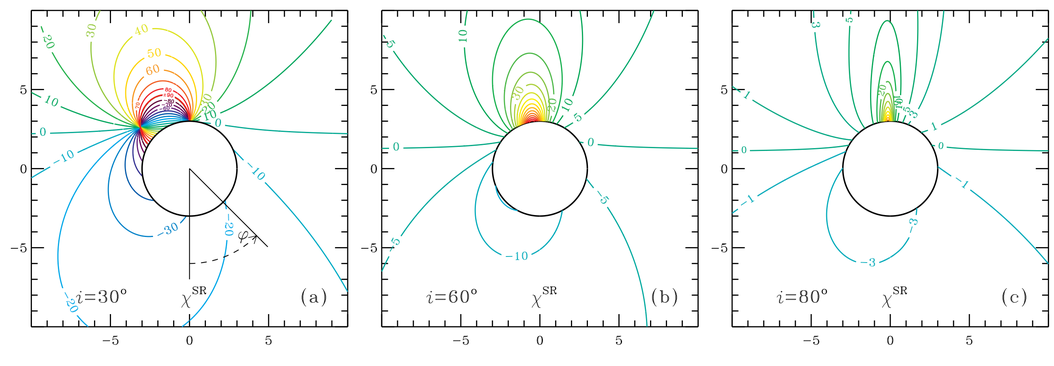

Figure 5: Same as Fig. 3 but for $\chi_{\rm SR}$.

We use approximate light-bending (ALB) expressions $\alpha(\psi)$ from Poutanen (2020) and it works exceptionally when compared with exact light-bending calculations. The topology of $\chi^{\rm tot}$ is shown in Fig. 3 as a map on the accretion disc plane in the form of contours of constant values. We see that for $i = 30°$ there exists a critical point (at $r \approx 4.06,\ \varphi \approx 230°$) where photons are emitted along with the disc normal in the comoving frame resulting in zero PD and not defined PA. At large inclinations, the strongest variations in PA are seen around $\varphi = 180°$. Calculations using the analytical ALB formula for light bending produce nearly identical pictures (see the dotted lines barely separable from the solid lines in Fig. 3).

The general topology of $\chi^{\rm tot}$ is easier to understand by looking separately at the topology of $\chi^{\rm GR}$ and $\chi^{\rm SR}$, which are presented in Figs. 4 and 5, respectively. The anti-symmetry of $\chi^{\rm GR}$ in φ and very small rotation angles around $\varphi \approx 0$ are clearly seen. For the $\chi^{\rm SR}$, we see the existence of the critical point at small inclinations outside $r = 3$. The peak in SR rotation is reached close to $\varphi = 180°$ and the effect of SR rotation decreases with the increasing inclination, similarly to the GR rotation angle.

In Fig. 6 we show the total PA rotation $\chi^{\rm tot}$ for different radii and inclinations, as well as the error on the PA computed using ALB, as compared to the exact, numerical solution. We see that the relativistic effects decrease with radius, as expected. The largest rotation of the PA is observed at smaller inclinations. The difference between the PA computed using ALB and accurately is always smaller than $\sim 0.^{\circ}6$.

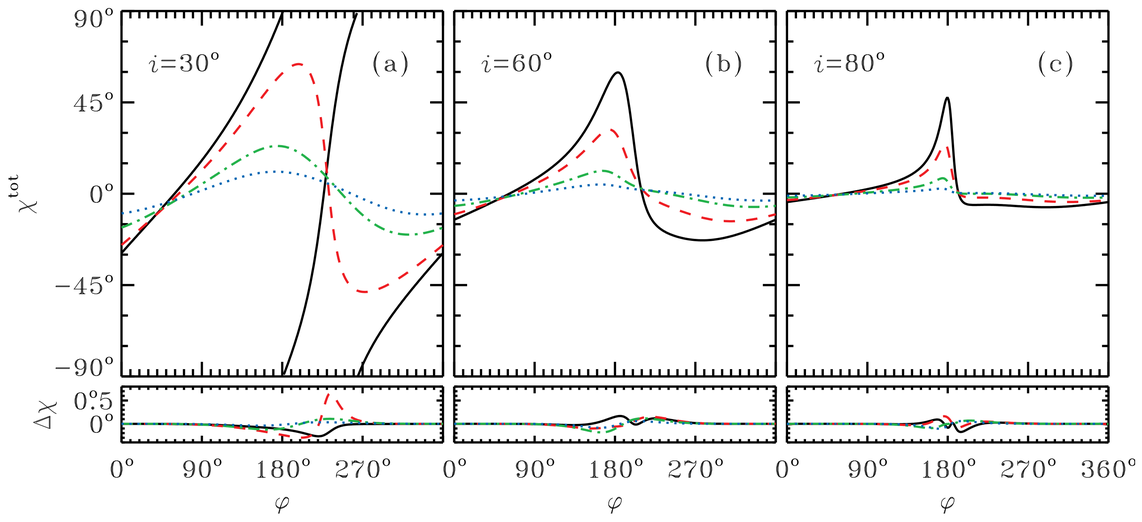

Figure 6: *Upper panels*: PA $\chi^{\rm tot}$ as a function of azimuth for disc inclinations $i = 30°$ (*panel a*), $60°$ (*b*) and $80°$ (*c*) and different $r = 3$ (black solid line), 5 (red dashed), 15 (green dot-dashed) and 50 (blue dotted). *Lower panels*: Difference in the PA rotation computed using ALB and via exact calculations.

Polarization of accretion disc

We compute the polarization signatures of the optically thick, geometrically (infinitely) thin accretion disc using the analytical formulae derived above. As an illustration, we consider the simple case of the standard accretion disc in Newtonian gravity (Shakura & Sunyaev 1973) and pure electron scattering atmosphere for polarization properties. Fig. 7 shows images of the accretion disc as viewed at three different inclinations.

Also in Fig. 7 we show the resulting spectral energy distributions of $x\,l_x$, PD (p) and PA (χ) for an accretion disc, as seen by a distant observer at different inclinations.The lower subpanels show the errors when computations are done using ALB. The integral flux has at most 1.5% relative error, owing to the fact that the error in lensing factor at different radii has different signs. Calculations using approximate formulae for light bending and lensing factor give very accurate results for polarization parameters, too. For example, the absolute error on PD is smaller than 0.03% for all inclinations and the error on the PA barely exceeds $0.^{\circ}1$.

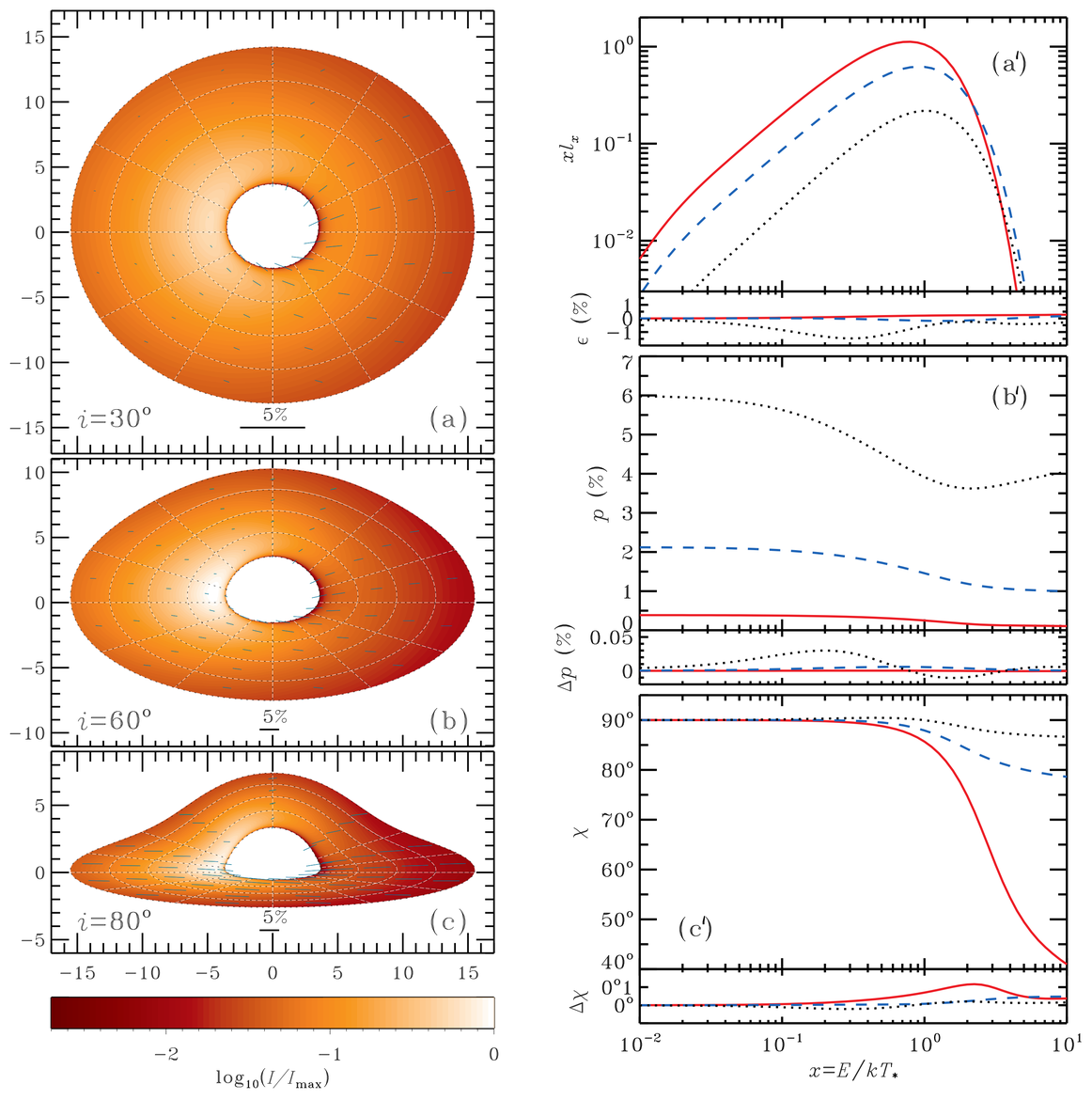

Figure 7: *Left panels:* Images of an accretion disc as viewed at three inclinations $i = 30°$ (*panel a*), $60°$ (*b*) and $80°$ (*c*). The coordinates on the sky are given in units of $R_{\rm S}$. Contours show the images of rings of equal radii r (from 3 to 15, with step of 3) and equal azimuths φ (every $30°$). Black solid contours correspond to the exact calculations of $\alpha(\psi)$, while the white dashed contours (almost fully overlapping with the black ones) are for ALB. The colours reflect the logarithm of the bolometric intensity. The blue sticks give polarization computed using ALB, with their length being proportional to the PD and their position angle is given by the PA. Exact calculations shown by green sticks are nearly indistinguishable from the approximation.
Right panels: Polarized spectrum of a standard accretion disc ($3 < r < 3000$) viewed at different inclinations: $i = 30°$ (red solid line), $60°$ (blue dashed), $80°$ (black dotted) as function of dimensionless photon energy $x = E/kT_*$, where $T_*^4 = \frac{3GM\dot{M}}{8\pi\sigma_{\rm SB}R_{\rm S}^3}$. *Panel a':* Normalized luminosity xl_x. *Panel b':* Polarization degree. *Panel c':* Polarization angle. The lower subpanels show the errors in the corresponding quantities when computations are done with ALB. Note that the error on xl_x is relative, while the errors on PA and PD are absolute.